Crack tip displacements of microstructurally small cracks in 316L steel and their dependence on crystallographic orientations of grains

I. SIMONOVSKI[1], KARL-FREDRIK NILSSON[2] and L. CIZELJ[1]

[1]*Jožef Stefan Institute, Reactor Engineering Division, Jamova 39, SI-1000 Ljubljana, Slovenia,* [2]*Institute for Energy, European Commission, DG-JRC, Postbus 2, 1755 ZG Petten, The Netherlands*

Received in final form XXX

ABSTRACT The paper presents an analysis of the effect of the grain orientations on a short Stage I surface crack in a 316L stainless steel. The analysis is based on a plane-strain finite element crystal plasticity model. The model consists of 212 randomly shaped, sized and oriented grains that is loaded monotonically in uniaxial tension to a maximum load of $1.12R_{p0.2}$ (280 MPa). The influence of random grain structure on a crack is assessed by calculating the crack tip opening (CTOD) and sliding displacements (CTSD) for single crystal and polycrystal models, considering also different crystallographic orientations. In the single crystal case the CTOD and CTSD may differ by more than one order of magnitude. Near the crack tip slip is activated on all the slip planes whereby only two are active in the rest of the model. The maximum CTOD is directly related to the largest Schmid factors. For the more complex polycrystal cases it is shown that certain crystallographic orientations result in a cluster of soft grains around the crack-containing grain. In these cases the crack tip can become a part of the localized strain, resulting in a large CTOD value. This effect, resulting from the overall grain orientations and sizes, can have a greater impact on the CTOD than the local grain orientation. On the other hand, when a localized soft response is formed away from the crack, the localized strain does not affect the crack tip directly, resulting in a small CTOD value. The resulting difference in CTOD can be up to a factor of 4, depending upon the crystallographic set. Grains as far as 6xCracklength significantly influence the crack tip parameters. It was also found that among grains with favourable orientation the CTOD increased with the size of such a grain. Finally, a significant change in CTOD and CTSD was observed when extending the crack into the second grain and placing it in the primary or the conjugate slip plane.

Keywords crack tip displacements; crystal plasticity; polycrystals; small cracks.

NOMENCLATURE

$\dot{a}^{(\alpha)}$ = reference strain rate
C_{ijkl} = stiffness tensor
CTOD = crack tip opening displacement
CTSD = crack tip sliding displacement
D = grain size
$\dot{g}^{(\alpha)}$ = current strain-hardened state
$h_{\alpha\alpha}$ = self-hardening moduli
$h_{\alpha\beta}$ = latent-hardening moduli
h_0 = initial hardening modulus
$m_i^{(\alpha)}$ = slip plane normal
n = strain-rate-sensitivity parameter

Correspondence : I. Simonovski. E-mail: igor.simonovski@ijs.si

q = hardening factor
$R_{p0.2}$ = yield stress
$s_i^{(\alpha)}$ = slip direction
$\dot{u}_{i,j}^p$ = plastic velocity gradient
(α) = index of active slip system
α = grain's crystallographic orientation
γ = cumulative slip
$\dot{\gamma}^{(\alpha)}$ = shear rate
ϵ_{kl}^e = elastic strain tensor
$<\epsilon_{ij}>$ = macroscopic strain
σ_{ij}^e = elastic stress tensor
$<\sigma_{ij}>$ = macroscopic stress
$\tau^{(\alpha)}$ = Schmid resolved shear stress
τ_s = reference stress
τ_0 = critical shear stress

INTRODUCTION

The behaviour of microstructurally small fatigue cracks distinctively differs from that of long cracks. In particular the average crack growth rate can be much higher for small cracks with equivalent crack tip loading (ΔK) as first discovered by Pearson[1] and they grow below threshold value for large cracks (ΔK_{th})[2].

Local propagation rate and path of small fatigue cracks is strongly affected by microstructural features such as grain boundaries, crystallographic orientations, inclusions, voids and material phases etc.[3–5] The microstructurally small cracks are often initiated from persistent slip bands and propagate along the slip planes. The crack tip loading is therefore generally mixed-mode and the crack changes direction as it passes through grain boundaries resulting in a serrated crack profile. Experimental data suggest that the fatigue crack growth rate and crack opening displacements tend to decrease when such cracks approach a grain boundary[5–7] and grain boundaries can also temporaryly block the plastic zone growth.[8] The difficulty in propagating slip across an interface may give rise to an incubation period that depends on the type of interface, e.g. high-angle grain boundary or interface with a second phase. Different crystallographic orientations of the grains may also increase, decrease or arrest the crack growth.[9,10] Vaek *et al.*[11] for example observed that crack propagation rates may vary significantly for nominally identical cracks. Crack closure and high strains can also play a significant role but plasticity induced crack closure effects are generally smaller for small cracks.[3,4,12]

Various models have been proposed to model the small crack behaviour. Obrtlík, Polák and Vaek[11,13] found that the propagation rate of microstructurally small cracks in 316L can be fitted to a power law for the plastic strain amplitude that is almost independent of the crack size. El Haddad *et al.*[14] could correlate short crack propagation of small cracks to experimental data fairly well by extending the physical crack length with the transition length, a_o, for small and long cracks defined by Kitagawa diagrams.[2] Grain boundary blocking models that assume that the slip band zone is blocked at a grain boundary until an effective stress intensity factor is attained have also been used successfully to model crack retardation and acceleration (see e.g. Ref. [15,16]). Alternatively the blocking is assumed to be related to the difference in crystallographic orientations between grains.[17] Other crack blocking models use separate equations and simply state that a long crack equation should be adopted if the threshold stress intensity factor is reached.[18]

In recent years several attempts have been made to model the behaviour of long cracks in single crystal[19] and small cracks in bicrystal[20] and polycrystals[21,22] using crystal plasticity material models but basically without the explicit grain shape modelling. Models with one, two[9,23,24] and more[24] explicitly modelled grains can be found in literature but they assume a rectangular grain shape. The misorientation between two grains was found to have a smaller influence on the crack tip displacements, crack propagation rates and crack tip plastic zone than assumed in grain blocking models and some experimental data.

The references above are, however, limited to a very simplified modelling of the grain shape itself. When one wants to extend the models to incorporate basic structural features such as large numbers of grains, we should as a first step also imitate the random shape and orientation of grains. These can have a significant effect on the crack tip parameters as shown by Ballarini *et al.* in Refs [25,26] where average values and standard deviations of stress intensity factors were calculated under the conditions of linear elastic fracture mechanics. Crystal plasticity was, however, not used. It is shown in Ref. [25] that the crack tip parameters are insensitive to the number of crystals and their orientation as long as the crack tip is surrounded by at least ten grains. Random grain geometry and crystal plasticity have been used inRef. [27] where

scatter of the $\mathcal{J}$-integral values has been determined for intergranular cracks.

In this paper, a model dealing with a fixed length, inclined small crack embedded in a surface grain of a plane strain polycrystal is proposed. Crack is embedded in an undamaged structure and subjected to monotonic loadings. The polycrystal assumes randomly shaped and oriented grains obeying anisotropic elasticity and crystal plasticity. The main intention of this study is to evaluate the influence that a random grain structure imposes on a Stage I crack. This is achieved by calculating crack tip opening (CTOD) and sliding (CTSD) displacements and analyzing their scatter for a number of cases where the crystallographic orientation of grains close and far from the crack tip is varied. Some results are presented using cumulative probability function. This method of presenting the results could lead to fundamental insight into the range of possible values, which can be attained experimentally. The reason behind using the crack tip opening displacement is that it (in combination with Paris law type equations) describes better the short crack propagation than stress intensity factors.[28] It also has the advantage of accounting for the mixed mode crack tip loading inherent in Stage I crack growth. The influence of the length of a crack and the proximity of the crack tip to the grain boundary are also investigated.

MODEL DESCRIPTION

Constitutive model

The elastic deformation at the monocrystal level is modelled using generalized Hooke's law, $\sigma^e_{ij} = C_{ijkl}\epsilon^e_{kl}$, where σ^e_{ij} represents the second-rank elastic stress tensor, C_{ijkl} the fourth-rank stiffness tensor and ϵ^e_{kl} the second-rank elastic strain tensor. The number of independent elastic constants for a cubic crystal system (BCC and FCC) is 3.

Crystal plasticity theory is used[29] to describe the material's plastic behaviour at the grain level. The plastic deformation in monocrystals is assumed to take place via a simple shear on a specific set of slip planes (see Fig. 1). Deformation by other mechanisms such as for example diffusion, twinning and grain boundary sliding is currently not taken into account. The combination of a slip plane, denoted by its normal m^α_i, and a slip direction, s^α_i, is called a slip system, (α). The plastic velocity gradient, $\dot{u}^p_{i,j}$, due to a crystallographic slip can be written as,

$$\dot{u}^p_{i,j} = \sum_\alpha \dot{\gamma}^{(\alpha)} s^{(\alpha)}_i m^{(\alpha)}_j, \tag{1}$$

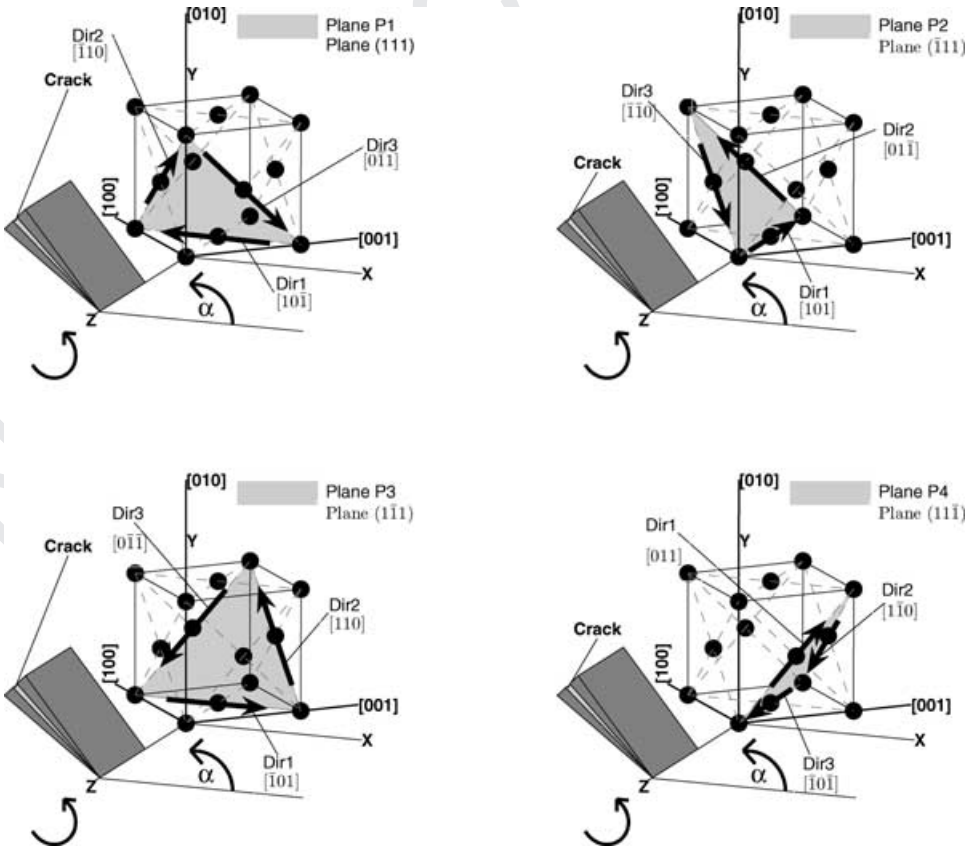

Fig. 1. Relation between the slip systems of a face centred cubic material and the crack for $\alpha = 0°$.

where the summation is performed over all active slip systems, (α), while $\dot{\gamma}^{(\alpha)}$ represents the shear rate. The cumulative slip, γ, is defined as,

$$\gamma = \sum_{\alpha} \int_0^t |\dot{\gamma}^{(\alpha)}|\, dt. \tag{2}$$

It is assumed that the shear rate $\dot{\gamma}^{(\alpha)}$ depends on the stress only via the Schmid resolved shear stress, Eq. (3). This is a reasonable approximation at room temperature and for ordinary strain rates and pressures. The Schmid resolved shear stress for a given slip system is given by Eq. (4). Yielding is then assumed to take place when the Schmid resolved shear stress exceeds the critical shear stress τ_0.

$$\dot{\gamma}^{(\alpha)} = \dot{a}^{(\alpha)} \left(\frac{\tau^{(\alpha)}}{g^{(\alpha)}} \right) \left| \frac{\tau^{(\alpha)}}{g^{(\alpha)}} \right|^{n-1} \tag{3}$$

$$\tau^{(\alpha)} = s_i^{(\alpha)} \sigma_{ij} m_j^{(\alpha)} \tag{4}$$

In eq. (3), $\dot{a}^{(\alpha)}$ represents the reference strain rate, n the strain-rate-sensitivity parameter and $g^{(\alpha)}$ the current strain-hardened state of the crystal. In the limit, as n approaches infinity, this power law approaches that of a rate-independent material. The current strain-hardened state $g^{(\alpha)}$ can be derived from,

$$\dot{g}^{(\alpha)} = \sum_{\beta} h_{\alpha\beta} \quad \dot{\gamma}^{(\beta)}, \tag{5}$$

where $h_{\alpha\beta}$ are the slip-hardening moduli defined by the adopted hardening law. In this work Peirce *et al.* hardening law is used,[30] where self-hardening moduli $h_{\alpha\alpha}$ are defined by:

$$h_{\alpha\alpha} = h_0 \mathrm{sech}^2 \left(\frac{h_0 \gamma}{\tau_s - \tau_0} \right), \quad \mathrm{sech} = 1/\cosh. \tag{6}$$

Here h_0 stands for the initial hardening modulus, τ_0 the yield stress (equal to the initial value of the current strength $g^{(\alpha)}$ (0)) and τ_s a reference stress where large plastic flow initiates.[31] The latent-hardening moduli $h_{\alpha\beta}$ are given by,

$$h_{\alpha\beta} = q h_{\alpha\alpha}, \qquad (\alpha \neq \beta), \tag{7}$$

where q is a hardening factor. This model was implemented as a user-subroutine into the finite element code ABAQUS.

Macroscopic stress $<\sigma_{ij}>$ and strain tensors $<\epsilon_{ij}>$ are estimated using volume averaging. For comparison with engineering stress and strain Mises equivalent stress and strain are used. Further details on its theory and implementation can be found in Refs [31,32].

Layout of structural model

The structural model is a planar rectangular aggregate with 212 randomly sized and shaped grains. The grain structure is a planar Voronoi tessellation generated using code VorTESS.[33] The finite element model of the grain structure with a crack is presented in Fig. 2.

Each grain is subdivided into 8-noded, reduced-integration, plane strain finite elements. The finite element meshing of the grains away from the crack tip is automatic and follows procedures outlined in Ref. [34]. To avoid violations of finite element shape constraints, only a subset of "meshable" Voronoi tessellations has been considered in the analysis. The "meshable" tessellations basically assume reasonably small aspect ratios of chord lengths. Further details are available in Ref. [34]. Such approach essentially prevents use of tessellations with very small grains. The finite element meshing of the crack tip neighbourhood is detailed in section titled 'the crack and the crack tip mesh'.

Each grain is assumed to behave as a randomly oriented monocrystal governed by the anisotropic elasticity and crystal plasticity models as described in the previous section. The number of grains included in the model is not sufficient to result in a size-independent macroscopic response of the aggregate (representative volume element). However, the experience with similar simulations shows that the error caused by this omission is limited to about 5 %.[32]

The average grain size of 52.9 μm is used in the analysis. This agrees well with values published for 316L steel being between 50 μm and 80 μm.

Crystallographic orientations

Appropriate crystallographic orientations are achieved in two steps:

1. In the first step the angle between the crystallographic [100] direction and the macroscopic X axis of all crystals in the model is set to 135 $^\circ$ as shown in Fig. 1. This results in a planar slip system model compatible with the planar macroscopic model. The resulting projections of the primary and conjugate slip planes are illustrated in Fig. 3.
2. In the second step, random orientation of grains is achieved by randomly rotating crystals around the global Z-axis. Uniform distribution with range 0 to 2π is used. Within the grain the initial crystallographic orientations are identical.

Application of the macroscopic tension in the X-direction results in macroscopic maximum shear stress planes at $\pm 45^\circ$ to the X-axis. Now, coincidence of

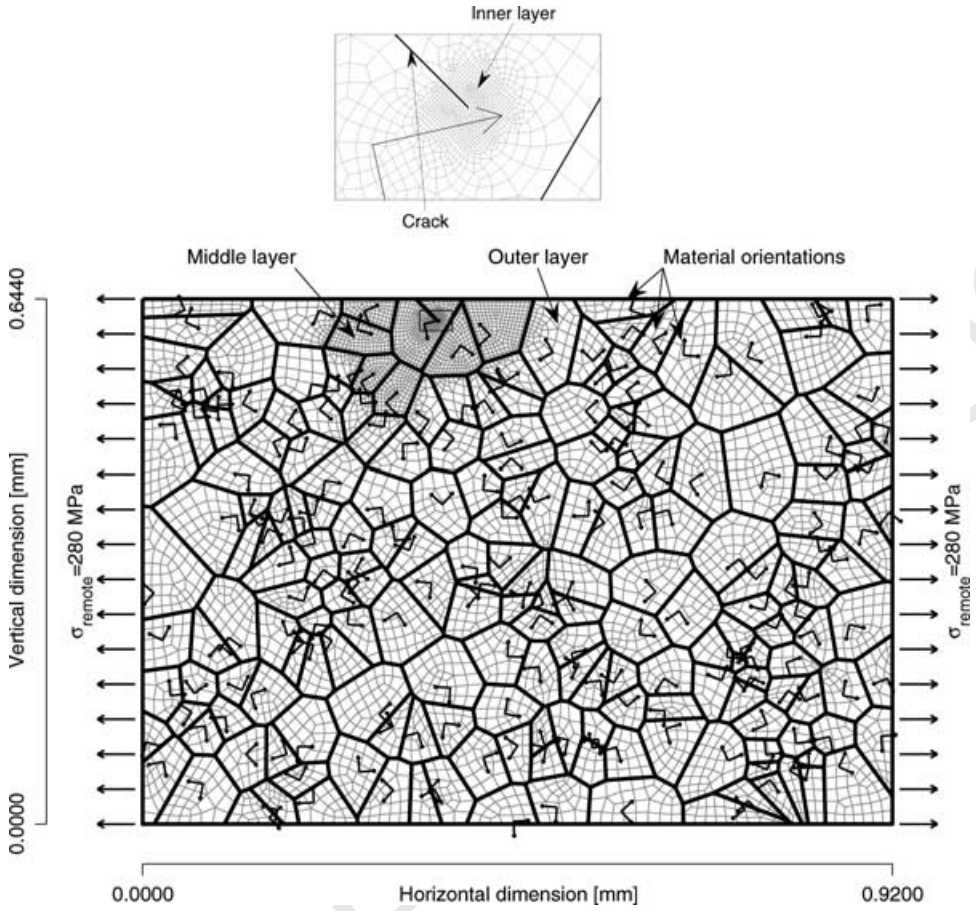

Fig. 2. The outline of the finite element model. Details of the crack tip meshing are shown in the insert.

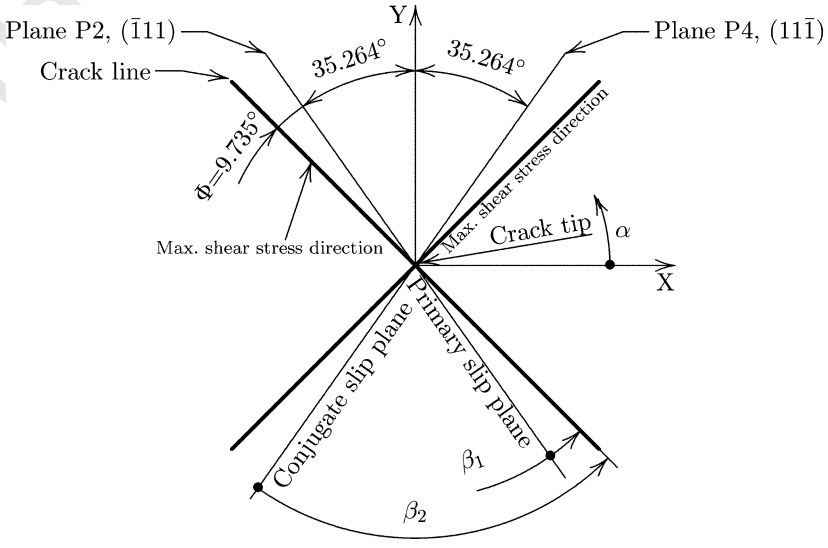

Fig. 3. Orientations of slip planes, shear directions and the crack plane for crystallographic orientation of $\alpha = 0^\circ$.

macroscopic shear planes and microscopic primary and conjugate slip planes is achieved when the crystals are rotated around the Z axis for: $\alpha = 9.735^\circ$, 80.265°, 99.735° or 170.265° as illustrated in Fig. 3.

Loading and boundary conditions

The applied macroscopic loading and boundary conditions are illustrated in Fig. 2. The left and right edges are loaded in macroscopic monotonic uniaxial tension up to

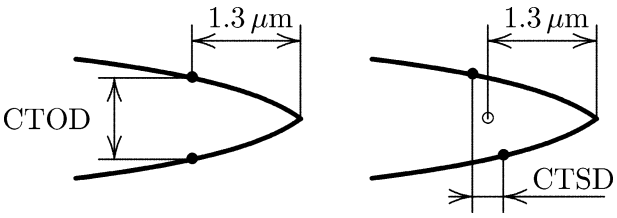

Fig. 4. Definition of the CTOD (left) and CTSD (right).

a maximum load of $1.12R_{p0.2}$ (280 MPa) with zero shear traction. This load is sufficient to trigger slip systems activity in all cases analyzed. The macroscopic yielding is achieved in most cases analyzed. The upper and lower edges are traction free. Prevention of rigid body movement is also imposed.

The crack and the crack tip mesh

A short inclined surface crack is introduced in the model with macroscopic crack orientation fixed to -45° relative to the global X axis. The CTOD and CTSD values are calculated at a distance of 2.5% of the average grain size behind the crack tip (i.e. $0.025 \cdot 52.9 = 1.3$ μm; see Fig. 4). This is consistent with examples found in Refs [23,24].

It is our intention to model a Stage I fatigue crack. This basically requires:

1 Placing the crack into the primary slip plane. This is achieved by setting the crystallographic orientation of the cracked grain to $\alpha = 9.735^\circ$.
2 A model of growing crack. The rather large complexity of including both crack growth and cyclic loading into the model is however avoided at this point in time and may be included in the model in the future. Nevertheless, a series of stationary crack lengths ranging from $0.2D_{38}$ to $0.77D_{38}$ has been analyzed to assess the influence of the crack length on the one hand and the effects of the grain boundary vicinity on the other hand. $D_{38} = 70.87$ μm is the size of the cracked grain, estimated as a square root of the grain's area. 38 stands for assigned grain number.

All results in this paper are therefore obtained assuming stationary crack and monotonic loading regime.

Extensive mesh sensitivity study was performed resulting in the optimal mesh shown in Fig. 2. The typical crack tip element size is about 0.25 μm. This mesh is expected to underestimate CTOD and CTSD for about 4.6% and 8.4%, respectively. This is deemed sufficient for this analysis. In cases where the crack is close to the grain boundary the size of the typical crack tip element has been halved.

Material parameters

The following elastic constants for AISI 316L single crystal are used: $C_{iiii} = 163680$ MPa, $C_{iijj} = 110160$ MPa, $C_{ijij} = 100960$ MPa.[35] Crystal plasticity parameters have been optimized from the macroscopic plastic response of AISI 316L polycrystal.[35] $b_0 = 330$ MPa, $\tau_s = 270$ MPa, $\tau_0 = 90$ MPa, $n = 55$, $q = 1.0$ and $\dot{a}^{(\alpha)} = 0.001$. With these parameters the proposed plain strain model is deemed sufficient to provide a correct qualitative representation of the macroscopic response.

RESULTS

The primary goal in this paper is to estimate the influence the random grain structure imposes on the CTOD and CTSD of the inclined short surface crack. Investigation is focused on the randomness of orientations while keeping the grain shapes constant. Such approach is expected to reveal most of the variability contributed by the random grain structure.[36]

Three main cases with inclined stationary short surface crack have therefore been analyzed:

1 Large monocrystal: the goal is to provide the dependence of CTOD and CTSD on the relative orientation between the crack and the crystal. Also, the orientations with extreme CTOD and CTSD values are revealed.
2 Large polycrystal: the scatter of CTOD and CTSD values due to the randomness of the grain structure is investigated.
3 Some specific configurations of grains in the vicinity of the crack have been analyzed to assess the relative influence of the close and far grains on the CTOD and CTSD.

Finally, the effects of the variations in the crack length and the vicinity of the grain boundary are analyzed for some typical configurations.

Large monocrystal

The finite element model of the large monocrystal configuration as shown in Fig. 2 and assumes a crack length of $0.5D_{38}$. Its geometric features are identical with the finite element models used in the polycrystalline cases. The crystallographic orientations are identical for all 212 grains. A series of analyses was performed with crystallographic orientations varying from 0 up to 180° in 2° increments.

The macroscopic strain $<\epsilon_{11}>$ is depicted as a function of the crystallographic orientation in Fig. 5 for two values of external load: below ($0.96R_{p0.2}$) and above ($1.12R_{p0.2}$) macroscopic yield strength. It should be noted here that the macroscopic yield strength $R_{p0.2}$ has been measured on an isotropic sample. Certain orientations of the

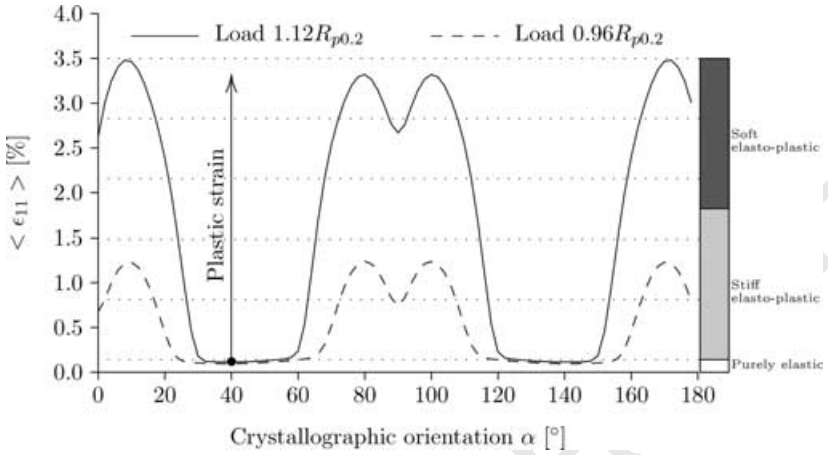

Fig. 5. Macroscopic strain $<\epsilon_{11}>$ as a function of the monocrystal's crystallographic orientation.

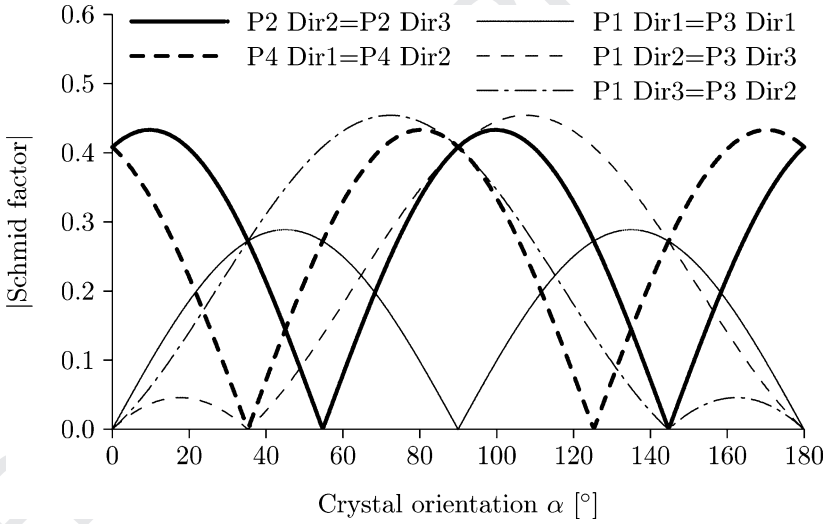

Fig. 6. Schmid factors as a function of the crystal orientation.

monocrystal are therefore not expected to yield macroscopically. We therefore classify the macroscopic strain $<\epsilon_{eq}>$ into three levels, which depend upon the crystallographic orientations: purely elastic, stiff elasto-plastic and soft elasto-plastic response. From now on we will refer to this classification as 'grain hardness index'. This will come in handy later on in the polycrystal configuration to display soft and hard grains.

Schmid factors for all the slip systems are depicted in Fig. 6. Comparing these factors with Fig. 5 one can, as expected, see that the maximal strains are obtained at crystallographic orientations where the Schmid factors on planes P2 (Dir2 and Dir3) and P4 (Dir1 and Dir2) are at their highest values as well. We will show later that, with the exception of the immediate vicinity of the crack tip, only these four slip systems are active in the model. Slip planes, directions and Miller indexes and vectors are shown in Fig. 1. The dominating crystal plasticity contribution to the macroscopic strain is clearly seen in Fig. 5 at the orientations $0 \leq \alpha \leq 30^\circ$, $60 \leq \alpha \leq 120^\circ$ and $150 \leq \alpha \leq 180^\circ$. The rest of the orientations exhibit significantly stiffer response dominated by the anisotropic elasticity. Substantial decrease in strain at $30 \leq \alpha \leq 60^\circ$ and $120 \leq \alpha \leq 150^\circ$ can be explained with smaller Schmid factors that in combination with the applied power law for calculating shear rate, Eq. (3), result in a significant reduction of the shear rate $\dot{\gamma}^{(\alpha)}$ and therefore shear as well. One can see that $<\epsilon_{11}>$ in Fig. 5 correlates very well with the cumulative slip, Eq. (2), recorded in finite elements far from the crack tip (Fig. 7). The same four slip systems are active in this case: P2 (Dir2 and Dir3) and P4 (Dir1 and Dir2). Activity of the rest of the slip systems is negligible. Near the crack tip more slip systems are activated and slip system activity is much more complex (Fig. 8). Slip systems P1, Dir1 and P3, Dir1 are activated in addition to the activated systems in elements far from the crack tip.

CTOD and CTSD at the load levels of $0.96R_{p0.2}$ and $1.12R_{p0.2}$ are depicted in Fig. 9 as a function of crystallographic orientation. The correlation between low CTOD regions and small cumulative slip regions (Fig. 8) is excellent. Furthermore, these regions coincide well with small $<\epsilon_{11}>$ regions (Fig. 5), and small Schmid factors (Fig. 6).

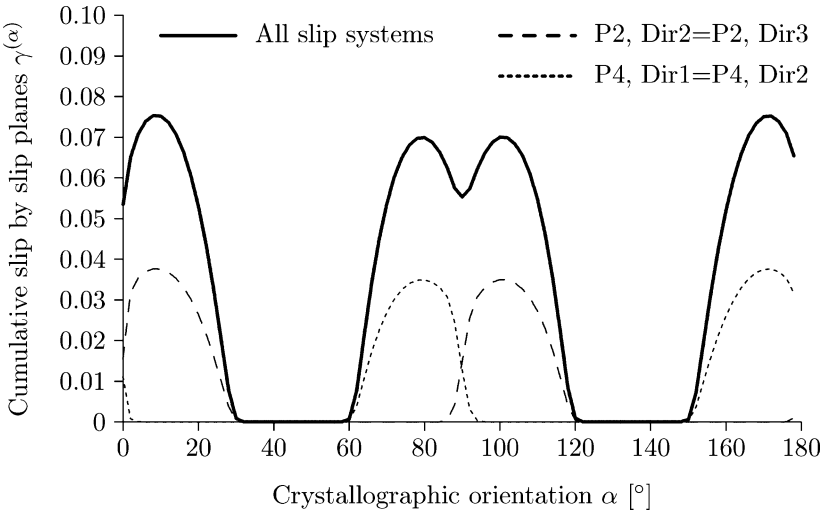

Fig. 7. The cumulative slip far from the crack tip for a single crystal configuration at different crystallographic orientations and load of $1.12R_{p0.2}$.

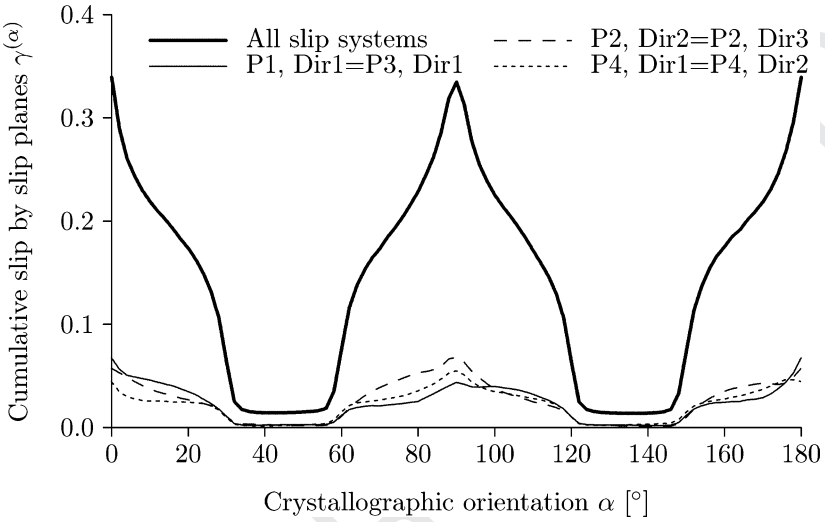

Fig. 8. The cumulative slip in the crack tip vicinity for a single crystal configuration at different crystallographic orientations and load of $1.12R_{p0.2}$.

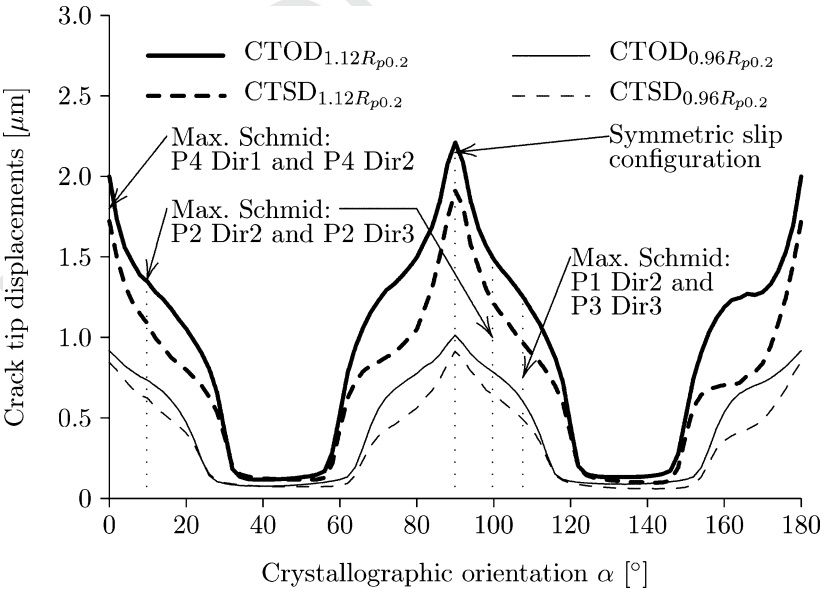

Fig. 9. Crack tip displacements as a function of the monocrystal's crystallographic orientation.

However, they are narrower. The largest crack tip displacements occur at crystallographic orientations where the Schmid factors are high. In these cases almost all part of a crack tip displacement is due to the plastic deformation. The largest crack tip displacements are at the crystallographic orientation that would result in symmetric slip at $\alpha = 90^\circ$ (note that the CTSDs are not zero since the crack is at an angle of 45°). This result is to some extent surprising, since we expected the CTOD and CTSD maxima for the crack in the slip plane ($\alpha = 9.735^\circ$ or $\alpha = 80.264^\circ$). However, for $\alpha = 90^\circ$ the most complex slip system activity is noted: active slip systems include P2 (Dir2 and Dir3) and P4 (Dir1 and Dir2) plus P1 Dir1 and P3 Dir1, all of them being close to the maximum Schmid factor (see Fig. 6). Since the activation of the slip systems other than the in plane P2 (Dir2 and Dir3) and P4 (Dir1 and Dir2) is to a large extent triggered by the local strain field and by the plane strain constraint, a future 3-D analysis will be needed to clarify this issue.

For the purpose of this paper and pending the 3-D resolution of local slip systems activity, the most unfavourable direction of the crack is in accordance with the Stage I crack assumed to be inline with the primary slip plane with respective crystallographic orientations of $\alpha = 9.735^\circ$. The most unfavourable direction for the crack is assumed to be at $\alpha = 135^\circ$. The respective CTOD values at $1.12R_{p0.2}$ are 1.34 μm and 0.13 μm. The extreme CTOD value of 2.21 μm has been, as already mentioned, recorded at the symmetric slip configuration at $\alpha = 90^\circ$.

Before embarking on the random polycrystalline case it was considered interesting to analyze also the behaviour of a large bicrystal. Based on above favourable and unfavourable configurations, a model of a bicrystal has been constructed as follows: the orientation of the crack containing grain was set to $\alpha = 9.735^\circ$ (Stage I crack) while all remaining grains were oriented at 135° to minimize CTOD as much as possible. This resulted in CTOD value of 0.158 μm, which is notably higher than obtained by orienting all the grains in the crack retardation orientation of 135° (0.116 μm). This indicates considerable importance of the orientation of the crack containing grain.

Polycrystal

The polycrystal case was simulated by applying 150 sets of random orientations to 211 out of the 212 grains in the model outlined in Fig. 2. The orientation of the crack containing grain was kept fixed to 9.735° in all simulated cases to mimic the Stage I crack aligned with the slip plane. The resulting cumulative probability of CTOD values is depicted in Fig. 10 with small + signs and labelled as '9.735, random' case. The computed CTOD values fall mainly in the middle of the monocrystal extreme values. The scatter of the results is completely attributed to the random orientations of the intact grains. Ninety-two per cent of all calculated CTOD values fall within the CTOD values of 0.4 μm and 1.1 μm, with average value at 0.765 μm.

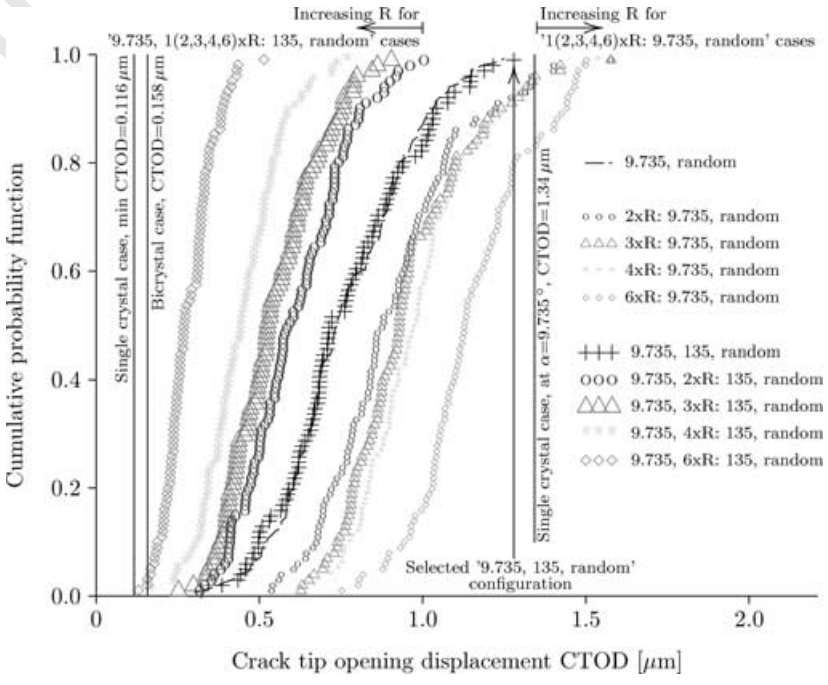

Fig. 10. Cumulative probability functions at a load of $1.12R_{p0.2}$.

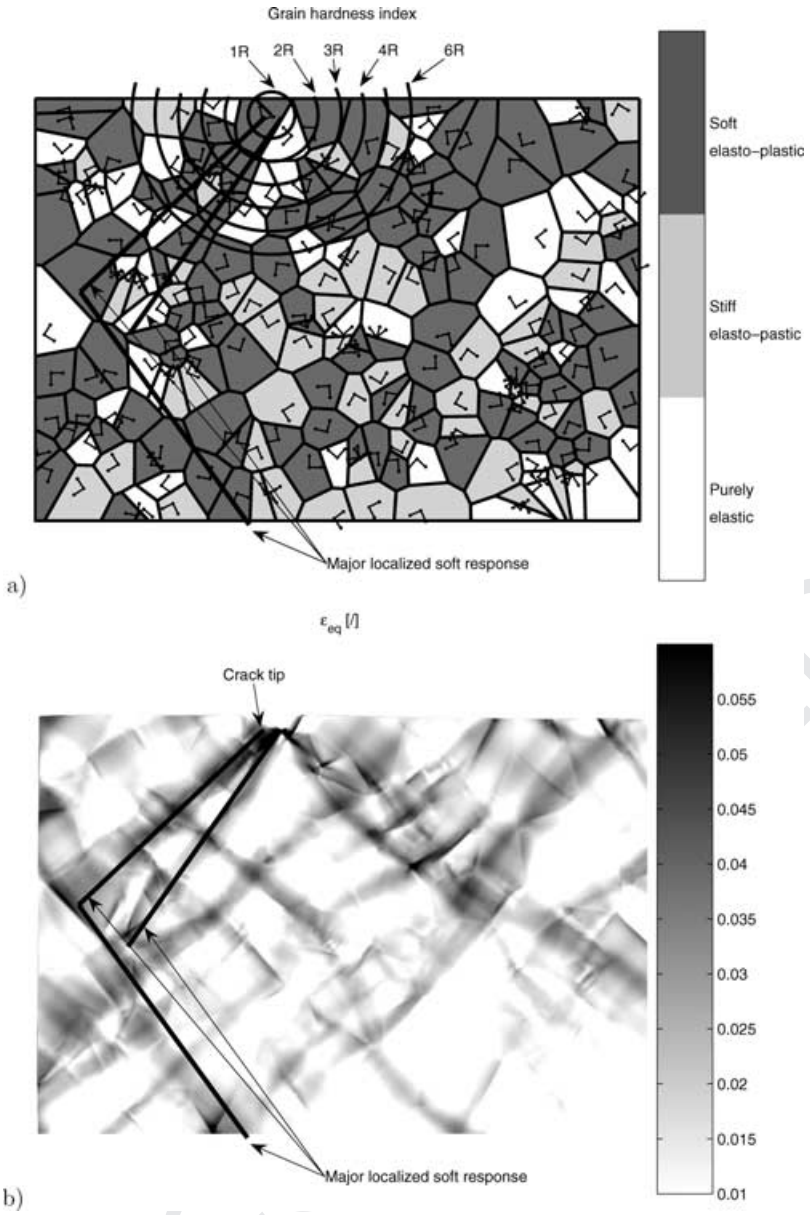

Fig. 11. Grain hardness index (a) and equivalent strain (b) for the '9.735, 135, random' crystallographic orientation set resulting in maximal CTOD.

The initial orientations of grains for the case with maximum and minimum CTODs are plotted in Figs 11 and 12, respectively, using the grain hardness index. The orientations are grouped to indicate three levels of monocrystal responses, as depicted in Fig. 5: purely elastic, stiff elasto-plastic and soft elasto-plastic. It is clear from Figs 11 and 12 that the magnitude of the CTOD strongly depends on the grain clusters with soft elasto-plastic response leading to a localized soft response (e.g., shear band) of the polycrystal. If such a cluster develops in crack vicinity, the crack tip becomes part of the localized strain, resulting in a large CTOD value (Fig. 11). On the contrary, when a soft cluster is formed away from the crack, the localized strain does not affect the crack tip directly, resulting in a small CTOD value (Fig. 12).

This indicates that the orientations of grains far away from the crack tip may contribute significantly to the development of localized strain patterns, which are significantly larger than the size of a typical grain. The position of localized strain patterns may in turn significantly influence the CTOD values.

Orientations of the crack containing grain and grains in its immediate vicinity

In addition to the localized strain patterns, the orientations of the crack containing grain and grains in its immediate vicinity are expected to have dominant effect on the development of the CTOD. Two sets of simulations have been performed to assess this effect:

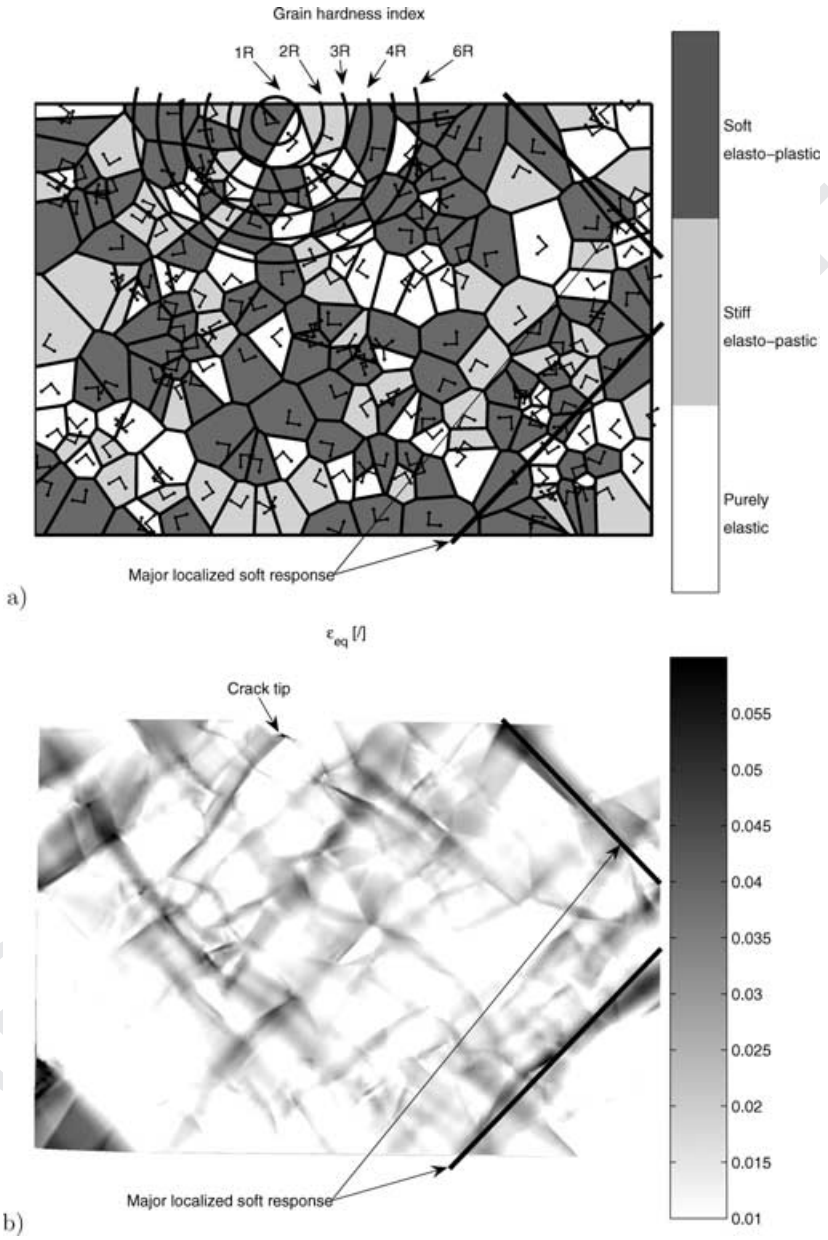

Fig. 12. Grain hardness index (a) and equivalent strain (b) for the '9.735, 135, random' crystallographic orientation set resulting in minimal CTOD.

'1(2,3,4,6)xR: 9.735, random' case. Increasing the size of the monocrystal containing the crack. This has been achieved by setting the orientation of the crack containing grain and all grains falling into radii of 2, 3, 4 and 6x crack lengths to $\alpha = 9.375^\circ$. All remaining grains assumed random orientation (100 different realizations). A notation of '3xR: 9.735, random' therefore means that all grains having their Poisson points (located in the centre of local coordinate systems) within radius of three times crack length (3xR) are oriented at 9.735°, while all other grains are oriented randomly. The radii are indicated in Fig. 11.

'9.735, 1(2,3,4,6)xR: 135, random' case. Increasing the size of the bicrystal with crack. The orientation of the crack containing grain was set to $\alpha = 9.375^\circ$, the orientation of the first neighbouring grain in the direction of the crack growth has been set to unfavourable $\alpha = 135^\circ$. The size of the unfavourably oriented (135) grain has then been increased by applying the $\alpha = 9.375^\circ$ orientation to all grains falling into radii of 2, 3, 4 and 6x crack lengths (with the exception of the crack containing grain). All remaining grains assumed random orientation (100 different realizations). A notation of '9.735, 3xR: 135, random' therefore means that the orientation of the first grain is

Table 1. Short statistics of the CTOD values

Case	CTOD [μm]			
	Min	Max	Mean	Std Dev
9.735, random	0.303	1.250	0.765	0.194
2R: 9.735, random	0.537	1.576	0.909	0.209
3R: 9.735, random	0.628	1.577	0.956	0.192
4R: 9.735, random	0.623	1.537	0.991	0.181
6R: 9.735, random	0.752	1.501	1.152	0.173
9.735, 135, random	0.323	1.280	0.763	0.205
9.735, 2R: 135, random	0.317	1.004	0.610	0.155
9.735, 3R: 135, random	0.252	0.904	0.546	0.139
9.735, 4R: 135, random	0.170	0.769	0.449	0.119
9.735, 6R: 135, random	0.130	0.515	0.284	0.074

9.735°, orientation of grains having their Poisson points within radius of three times crack length (3xR) is 135°, while all other grains are oriented randomly.

We expect the results to tend towards the single crystal case, however, the calculations will show the range of scatter and are also useful for understanding more complex cases.

Figure 10 shows the cumulative probability functions for the above cases. Min/max CTOD values for a limiting case of a single crystal are plotted for comparison. Also, the CTOD value for a bicrystal case (crack-containing grain: $\alpha = 9.375°$, all other grains: $\alpha = 135°$) is shown. One can see that for the '9.735, random' case the random crystallographic orientation can change the CTOD by a factor of 4 (c.f. Table 1). If we consider the values from all the analyzed cases, the ratio CTODmax/CTODmin increases to 11.8. Increasing the size of the crack-containing monocrystal to 2, 3, 4, 6xR gradually increases the CTOD, but the spread of the values does not decrease significantly. It is interesting to note that the impact of the monocrystal size vanishes at large CTOD values, where cumulative densities of 2, 3, 4 and 6xR overlap. This indicates that in this region the CTOD is dominated by the localized high strain areas (areas of grains with favourable orientation in the direction of maximum shear). Monocrystal size of 6xR is the maximal size considered to avoid significant effects from the model size. Model with more grains would have to be employed to investigate this matter further in the future. It is also interesting to note that the max. CTOD can actually be higher than of a limiting case of a single crystal. We attribute this to the occurrence of localized high strain areas in the polycrystal case.

As expected, increasing the size of the $\alpha = 135°$ layer ('9.735, xR: 135, random' case) around the crack-containing grain decreases the CTOD values. The limit case in this situation is the bicrystal case. The spread of the CTOD values here gradually decreases and max/min

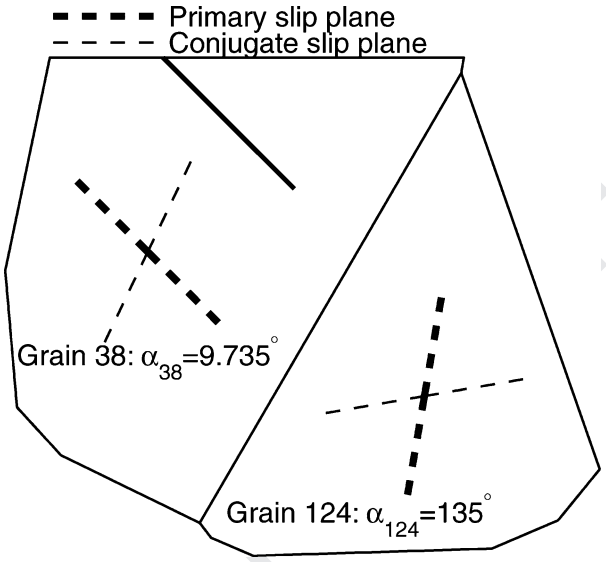

Fig. 13. Grain numbering with indicated directions of primary and conjugate slip planes.

CTOD ratio is still 3.8 at '9.7356, 6xR: 135, random' case. In this case the structure beyond 6xR significantly affects the CTOD values as well. It is also noted that the bicrystal configuration successfully minimizes the effects of the localized high strain areas due to its high stiffness.

CTOD and CTSD for different crack lengths

The influence of the crack length has been assessed by studying a series of stationary cracks with lengths ranging from $0.2D_{38}$ to $0.77D_{38}$. At $0.7403D_{38}$, the crack tip is at the grain boundary. The considered variations in crack length therefore noticeably changes the distance of the crack tip to the grain boundary, represented by an abrupt discontinuity of the material orientations. No attempt has been made in this paper to distinguish the potential influence of the grain boundary from the effects resulting from crack length variations.

The full statistical analysis taking into account a sufficient number of random grain orientations seemed exhaustive in terms of computational resources and was therefore not attempted. The orientations of grains in the model have been chosen to maximize the change in CTOD while approaching the grain boundary. To this end, the crack was aligned with the slip system in the first grain $\alpha = 9.735°$ (numbered as grain 38 in Fig. 13), while the second grain (numbered as grain 124 in Fig. 13) was oriented to $\alpha = 135°$ in order to minimize the CTOD in the second grain. For the rest of the grains, random orientations resulting in the absolute maximum of CTOD was selected. This set of orientations is depicted in Fig. 11 while Fig. 13 shows the orientations for the two grains involved. In order to minimize potential numerical

problems for the crack tip approaching the grain boundary (= discontinuity in material orientation), the size of a typical crack tip element was reduced to 0.125 μm.

The results for the elastically dominated case with remote load of $0.5R_{p0.2}$ are shown in Fig. 14. A monotonic increase in the CTOD with increasing crack length until the grain boundary is reached confirms that the CTOD behaviour is dominated by the elastic response. The limited activity of slip systems however shows a slightly more pronounced effect on the CTDS, which reaches its maximum value well before the crack tip reaches the grain boundary. Slight decrease in CTSD just before the grain boundary indicates that the activity of the slip systems has been hindered by the grain boundary. Immediately after the crack tip passes the grain boundary, a 9.4% decrease in CTOD is recorded.

The results for crystal plasticity dominated response at remote load of $1.12R_{p0.2}$ are depicted in Figs 15 and 16.

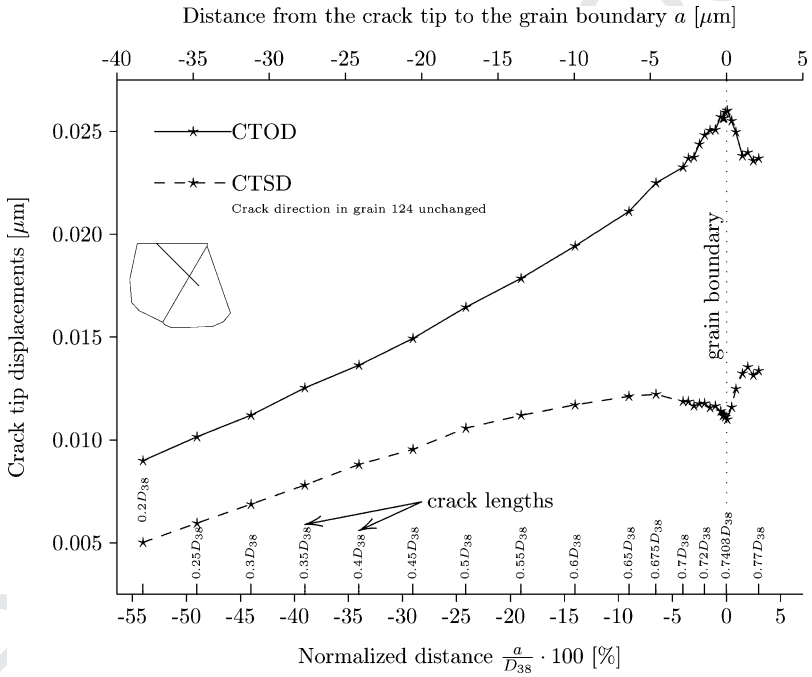

Fig. 14. The influence of crack length and proximity to the grain boundary on the crack tip displacements. Remote load $0.5R_{p0.2}$.

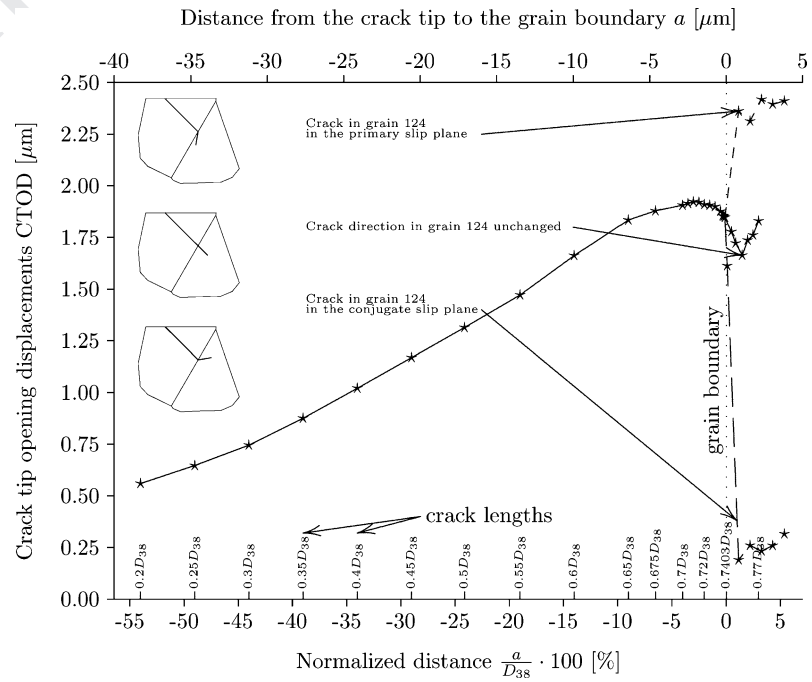

Fig. 15. The influence of crack length and proximity to the grain boundary on the crack tip opening displacements. Remote load $1.12R_{p0.2}$.

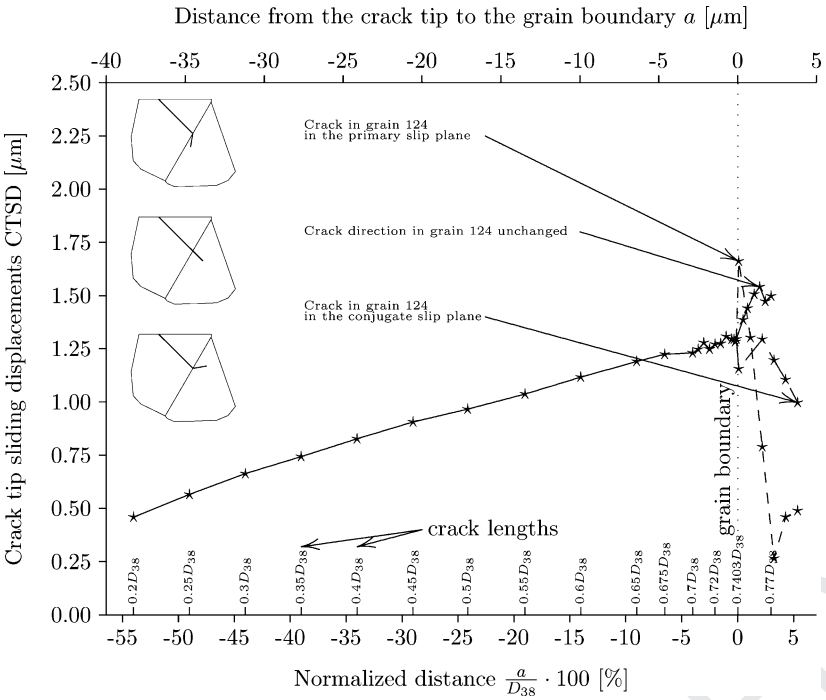

Fig. 16. The influence of crack length and proximity to the grain boundary on the crack tip sliding displacements. Remote load $1.12R_{p0.2}$.

The monotonic increase of CTOD with crack length is blocked by the noticeable slip system activity at crack length of $0.7D_{38}$. Further increase of the crack length causes the interaction of the slip system activity with the grain boundary, resulting in the decrease of the CTOD. The maximum drop of CTOD of 12.7% is noted immediately after the crack tip passes the grain boundary. Given the large influence of the crystallographic orientations on the CTOD and CTSD in a monocrystal configuration, a more pronounced grain boundary effect was expected. Similar results have, however, been reported by Potirniche *et al.*[23] At this load results are also presented for crack extension kinked into the primary/conjugates slip plane in accordance with Stage I. One can see that placing the crack extension into the primary slip plane significantly increases CTOD and decreases the CTSD. The reason for this is that the crack is now closer to the opening mode (Mode I). Opposite trend is observed for the CTOD when the crack extension is placed into the conjugate slip plane. In this case the CTSD still decreases after the grain boundary but significantly less then for the crack extension placed into the primary slip plane.

The possible reasons for unexpectedly small retardation of CTOD and CTSD while crack approaches the grain boundary include application of simple monotonic loading and possibly oversimplified modelling of grain boundaries (e.g., only discontinuity of material orientations) and will be further investigated in the future.

FUTURE WORK

Although a number of conclusions can be drawn from the results of the paper several issues can not be fully closed. One of them is certainly the question of the slip activity close to the crack tip in a fully 3D environment. Would that in the single crystal case result in attaining the max CTOD when the crack is aligned with the primary(secondary) slip plane instead as now when we have symmetric slip at $\alpha = 90°$? Another open question is what kind of combination of grain orientations and sizes results in localization of the strain (shear band) around the crack tip that increases the CTOD. We have shown that these localizations significantly affect the CTOD, even to the point where the size of the crack-containing grain did not significantly influence the CTOD. And finally, we need to incorporate cyclic loading and use a suitable crack growth criteria for advancing the crack.

CONCLUSIONS

This paper proposes a crystal plasticity model where distribution of grain shapes and crystallographic orientations are accounted for. It is shown that these significantly influence the crack tip displacements.

Although the loading in this paper is monotonic, a number of key observations are still relevant for the fatigue case. For a single crystal case the following conclusions can be drawn:

- CTOD closely follows maximal Schimdt factors on P2 and P4 planes.
- Maximal CTOD is obtained at symmetric crystallographic orientation of $\alpha = 90^\circ$ when six slip systems are activated in the crack tip vicinity.
- Near the crack tip slip is activated on all the slip planes whereby only two are active in the rest of the model (P2 and P4).

For the polycrystal case we have shown that a cluster of soft grains can lead to a localized soft response (e.g., shear band) of the polycrystal. If such a cluster develops in crack vicinity, the crack tip becomes part of the localized strain, resulting in a large CTOD value. This effect, resulting from the overall grain orientations and sizes, can have a greater impact on the CTOD than the local grain orientation. On the other hand, when a localized soft response is formed away from the crack, the localized strain does not affect the crack tip directly which results in a small CTOD value. The influence of the microstructure therefore has a significant impact on the crack. Overall, the difference in CTOD can reach a factor of 4. Even the grains beyond 6xCrackLength significantly influence the crack tip parameters. Further work is needed to assess how far this influence reaches. It was also found that among grains with favourable orientation the CTOD increased with the size of such a grain. Amongst all the surface grains the largest favourable oriented grains would therefore be more susceptible of faster crack propagation.

Finally, smaller than expected drop in the CTOD and CTSD was obtained as the crack approached the grain boundary. This could be due to the assumption of the unchanged crack direction, only monotonic loading and simplified grain boundary modelling. Significant change in the CTOD and CTSD was, however, observed when the crack extension in the second grain was placed in the primary or the conjugate slip plane.

Acknowledgements

XXX

REFERENCES

1 Pearson, S. (1975) Initiation of fatigue cracks in commercial aluminum alloys and the subsequent propagation of very short cracks. *Eng. Fract. Mech*. **7**, 235–247.
2 Kitagawa, H. and Takahashi, S. (1976) Applicability of fracture mechanics to very small cracks or the cracks in the early stage. *Proceedings of Second International Conference on Mechanical Behavior of Materials*, *ASM*, *Boston*, 627–631.
3 Miller, K. J. (1987) The behaviour of short fatigue cracks and their initiation. Part II-A general summary. *Fatigue Fract. Eng. Mater. Struct*. **10**, 93–113.
4 Hussain, K. (1997) Short fatigue crack behaviour and analytical models: A review. *Eng. Fract. Mech*, **58**, 327–354.
5 Hussain, K., delos Rios, E. and Navarro, A. (1993) A two-stage micromechanics model for short fatigue cracks. *Eng. Fract. Mech*, **44**, 425–436.
6 Morris, W. L., Buck, O., and Marcus, H. L. (1976) Fatigue crack initiation and early propagation in Al 2219-T851. *Metall. Trans. A.* **7A**, 1161–1165.
7 Blochwitz, C., Tirschler, W. and Weidner, A. (1982) The growth of small fatigue cracks in 7075-T6 aluminium alloy. *Fatigue Eng. Mater. Struct.* **5**, 233–248.
8 Morris, W. L. (1980) The noncontinuum crack tip deformation behavior of surface microcracks. *Metall. Trans. A.* **11A**, 1117–1123.
9 Tvergaard, V., Wei, Y. and Hutchinson, J. W. (2001) Edge cracks in plastically deforming surface grains. *Eur. J. Mech. A Solids* **20**, 731–738.
10 Zhai, T., Wilkinson, A. J. and Martin, J. W. (2000) A crystallographic mechanism for fatigue crack propagation through grain boundaries. *Acta Mater.* **48**, 4917–4927.
11 Vaek, A., Polák, J. and Obrtlík, L. (1996) Fatigue damage in two-step loading of 316L steel. II. Short crack growth. *Fatigue Fract. Eng. Mater. Struct.* **19**, 157–163.
12 Newman, J. C. J., Phillips, E. P. and Swain, M. H. (1999) Fatigue-life prediction methodology using small-crack theory. *Int. J. Fatigue* **21**, 109–119.
13 Polák, J., Obrtlík, K. and Vaek, A. (1997) Short crack growth kinetics and fatigue life of materials. *Mater. Sc. Eng. A* **234-236**, 970–973.
14 Haddad, M. El., Smith, K. and Topper, T. (1979) Fatigue crack propagation of short cracks. *J. Eng. Mater. Techn.-Transactions of The ASME* **101**, 42–46.
15 Tanaka, K., Akiniwa, Y., Nakai, Y. and Wei, R. (1986) Modelling of small fatigue crack growth interacting with grain boundary. *Eng. Fract. Mech*. **24**, 803–819.
16 Navarro, A., de los Rios, E. (1988) A microstructurally-short fatigue crack growth equation. *Fatigue Fract. Eng. Mater. Struct.*, **11**, 383–396.
17 Chan, K. S. and Lankford, J. (1983) A crack-tip strain model for the growth of small fatigue cracks. *Scripta Metallurgica*, **17**, 529–532.
18 Hobson, P. D. (1982) The formulation of a crack growth equation for short cracks. *Fatigue Eng. Mater. Struct.* **5**, 323–327.
19 Rice, J. R., Hawk, D. E. and Asaro, J. R. (1990) Crack tip fields in ductile crystals. *Int. J. Fract.* **42**, 301–321.
20 Kysar, J. (2000) Directional dependence of fracture in copper sapphire bicrystal. *Acta Mater.* **48**, 3509–3524.
21 Gall, K., Sehitoglu, H. and Kadioglu, Y. (1996) Plastic zones and fatigue-crack closure under plane-strain double slip. *Metall. Mater. Trans. A* **27A**, 3491–3501.
22 Potirniche, G. P., Daniewicz, S. R. and Newman, J. C. Jr (2004) Simulating small crack growth behaviour using crystal plasticity theory and finite element analysis. *Fatigue Fract. Eng. Mater. Struct.* **27**, 59–71.
23 Potirniche, G. P. and Daniewicz, S. R. (2003) Analysis of crack tip plasticity for microstructurally small cracks using crystal plasticity theory. *Eng. Fract. Mech.* **70**, 1623–1643.
24 Bennett, V. P. and McDowell, D. L. (2003) Crack tip displacements of microstructurally small surface cracks in single phase ductile polycrystals. *Eng. Fract. Mech.* **70**, 185–207.
25 Ballarini, R., Mullen, R. L. and Heuer, A. H. (1999) The effects of heterogenity and anisotropy on the size effect in cracked polycrystalline films. *Int. J. Fract.* **95**, 19–39.

26 Wang, Y. and Ballarini, R. (2002) A long crack penetrating a circular inhomogenity. *Meccanica* **38**, 579–593.

27 Cizelj, L. and Riesch-Oppermann, H. (2002) Towards growth model for short intergranular cracks in elastoplastic polycrystalline aggregate. *Proceedings Fontevraud 5: International symposium Contribution of Materials Investigation to the Resolution of Problems Encountered in Pressurized Water reactors*, **1**, 96–203.

28 Blochwitz, C., Tirschler, W. and Weidner, A. (2003) Crack opening displacements and propagation rate of microstructurally short cracks. *Mater. Sc. Eng. A* **357**, 264–269.

29 Hill, R. and Rice, J. R. (1972) Constitutive analysis of elastic-plastic crystals at arbitrary strain. *J. Mech. Phys. Solids.* **20**, 401–413.

30 Peirce, D., Asaro, R. J. and Needleman, A. (1983) Material rate dependence and localized deformation in crystalline solids. *Acta Metall.* **31**, 1951–1976.

31 Huang, Y. (1991) A user-material subroutine incorporating single crystal plasticity in the ABAQUS finite element program. *Mech Report 178*, Division of Applied Sciences, Harvard University.

32 Kova, M. and Cizelj, L. (2005) Modeling elasto-plastic behavior of polycrystalline grain structure of steels at mesoscopic level. *Nucl. Eng. Des.*, **235**, 1939–1950.

33 Riesch-Oppermann, H. (1999) Generation of 2–D random Poisson–Voronoi mosaics as framework for micromechanical modeling of polycrystalline materials-algorithm and subroutines description. *Tech. Rep. FZKA 6325*, Forschungszentrum Karlsruhe.

34 Weyer, S., Fröhlich, A., Riesch-Oppermann, H., Cizelj, L. and Kova, M. (2002) Automatic finite element meshing of planar Voronoi tessellations. *Eng. Fract. Mech*, **69**, 945–958.

35 Simonovski, I., Nilsson, K. F. and Cizelj, L. (2005) Material properties calibration for 316L steel using polycrystalline model. 13th International Conference On Nuclear Engineering, Beijing, China,

36 Weyer, S. (2001) Experimentelle Untersuchung und Mikromechanische Modellierung des Schädigungsverhaltens von Aluminiumoxid unter Druckbeanspruchung. *Ph.D. thesis*, Universität Karlsruhe.

Author Query Form

Journal: FFE
Article: ffe1098

Dear Author,
During the copy-editing of your paper, the following queries arose. Please respond to these by marking up your proofs with the necessary changes/additions. Please write your answers on the query sheet if there is insufficient space on the page proofs. Please write clearly and follow the conventions shown on the attached corrections sheet. If returning the proof by fax do not write too close to the paper's edge. Please remember that illegible mark-ups may delay publication.

Query Refs.	Query	Remarks
1	Author: Please check the author name 'de los Rios E' in refs 5 and 16.	

MARKED PROOF

Please correct and return this set

Please use the proof correction marks shown below for all alterations and corrections. If you wish to return your proof by fax you should ensure that all amendments are written clearly in dark ink and are made well within the page margins.

Instruction to printer	*Textual mark*	*Marginal mark*
Leave unchanged	··· under matter to remain	New matter followed by or or
Insert in text the matter indicated in the margin		
Delete	through single character, rule or underline or through all characters to be deleted	or
Substitute character or substitute part of one or more word(s)	through letter or through characters	new character or new characters
Change to italics	under matter to be changed	
Change to capitals	under matter to be changed	
Change to small capitals	under matter to be changed	
Change to bold type	under matter to be changed	
Change to bold italic	under matter to be changed	
Change to lower case	Encircle matter to be changed	
Change italic to upright type	(As above)	
Change bold to non-bold type	(As above)	
Insert 'superior' character	through character or where required	or under character e.g. or
Insert 'inferior' character	(As above)	over character e.g.
Insert full stop	(As above)	
Insert comma	(As above)	
Insert single quotation marks	(As above)	or and/or or
Insert double quotation marks	(As above)	or and/or or
Insert hyphen	(As above)	
Start new paragraph		
No new paragraph		
Transpose		
Close up	linking characters	
Insert or substitute space between characters or words	through character or where required	
Reduce space between characters or words	between characters or words affected	